A Landsat-era (1985-2015) Sierra Nevada (USA) Snow Reanalysis Dataset

MANUELA GIROTTO[1,2], STEVEN A. MARGULIS[3], GONZALO CORTÉS[3], LAURIE S. HUNING[3], DONGYUE LI[4], AND MICHAEL DURAND[4]

ABSTRACT

This work presents a newly developed state-of-the-art snow water equivalent (SWE) reanalysis dataset over the Sierra Nevada (USA) based on the assimilation of remotely sensed fractional snow covered area data over the Landsat 5-8 record (1985-2015). The method (fully Bayesian), resolution (daily, 90-meter), temporal extent (31 years), and accuracy provide a unique dataset for investigating snow processes to ultimately improve real-time streamflow predictions of snow-dominated regions. The reanalysis dataset was used to characterize SWE climatology to provide a basic accounting of the stored snowpack water in the Sierra Nevada over the last 31 years. The ongoing California drought contains the lowest snowpack years (water years 2014 and 2015) and three of the four driest years over the reanalysis record. In particular, water year 2015 was a truly extreme (dry) year, with range-wide peak snow volume characterized by a return period of over 600 years.

Keywords: Snow Reanalysis, Sierra Nevada, Data Assimilation, Landsat

INTRODUCTION

In the Sierra Nevada, snowmelt accounts for over 70% of the total streamflow (Stewart et al., 2004), where the measured 1 April snow water equivalent (SWE) has long been used as a proxy for available dry-season water supply. California is currently experiencing a record-setting multiyear drought that started in 2012 (Famiglietti, 2014; Mao et al., 2015; Belmecheri et al., 2016), which has significantly impacted all aspects of water resources, including snowpack. The ongoing drought has led to acute water shortages, groundwater overdraft, critically low streamflow, and enhanced wildfire risk (Christian-Smith et al., 2014). Further, snow plays a key role in the montane energy balance because of its high albedo, and ecological systems and biogeochemical processes are highly sensitive to variability in the montane hydrologic cycle (Bales et al. 2006; Trujillo et al. 2012).

---

[1] Global Modeling and Assimilation Office, NASA Goddard Space Flight Center, Greenbelt, MD, USA
[2] GESTAR, Universities Space Research Association, Columbia, MD 21044, USA
[3] Department of Civil and Environmental Engineering, University of California, Los Angeles, CA, 90095
[4] School of Earth Sciences and Byrd Polar and Climate Research Center, The Ohio State University, Columbus, OH, 43210

Highly variable spatial and temporal patterns in snow cover are the result of complex montane topography and orographic effects and equally complex atmospheric circulation patterns (e.g., Dettinger et al. 2004; Lundquist et al. 2010) that influence both accumulation and melt spatial variability. Yet, most mountain regions remain undersampled with respect to in situ data. Based on the limited in situ data, we argue that significant strides in our understanding of snow processes in montane regions could be made using a regional reanalysis-type approach that merges information from uncertain model estimates and globally available remote sensing measurements to derive spatially and temporally continuous estimates over long periods.

The reanalysis approach we present in this document is focused specifically on snow and it is based on the leveraging of long-term 1984-2015 Landsat fractional snow- covered area (fSCA) datasets together with meteorological reanalysis products and snow modeling, merging all information streams within a fully Bayesian data assimilation framework. This document reports some key results taken entirely from the work by Margulis et al., (2016a, 2016b). In particular, we aim to give an overview about the reanalysis dataset, its validation, and the illustration of its utility in the context of characterizing snow climatology especially in the contest of the recent multiyear drought.

DATA AND METHODS

Landsat-Era Sierra Nevada Snow Reanalysis

Please refer to Margulis et al. (2015) for details of the methods used in this work. The primary data set used is the newly developed state-of-the-art snow reanalysis for the Sierra Nevada in the Western U.S. The reanalysis dataset is presented in Margulis et al. (2016a). The reanalysis method consists of a fully Bayesian data assimilation technique, which generates an ensemble posterior SWE estimate, based on a prior estimate from a land surface model (LSM) with a snow depletion curve (SDC), and remotely sensed fSCA observations that are used to condition (update) the prior estimate. The prior estimate leverages high-resolution elevation and land-cover data as static inputs, and downscaled meteorological forcing (Girotto et al. 2014; Margulis et al. 2015) as dynamic inputs, to generate high-resolution ensemble SWE and fSCA estimates over the full water year (WY; from 1 October to 30 September). Modules were developed and applied to account for the uncertainty in key model inputs, including the downscaled meteorological forcings. The forward model used in this study was the Simplified Simple Biosphere (SSiB; Xue et al. 2003) land surface model coupled to the Liston (2004) snow depletion model. The retrieved fSCA estimates used for assimilation in this study were derived from Landsat 5 Thematic Mapper (TM), Landsat 7 Enhanced Thematic Mapper (ETM1), and Landsat 8 Operational Land Imager (OLI) reflectance data using a spectral end-member unmixing approach based on Painter et al. (2003) and Cortés et al. (2014).

RESULTS

Validation of the Snow Reanalysis

The details of the snow reanalysis verification statistics can be found in Margulis et al., (2016a), only key statistics are reported in this document.

The data used for verification are in situ SWE data taken from 108 snow pillow and 202 snow course sites scattered across the Sierra Nevada. We found that posterior SWE estimates are generally significantly improved over the prior estimates in terms of mean error (ME), root-mean-square error (RMSE), and correlation coefficient when compared to the in situ data. The posterior ME values for snow pillows range across the basins from -12 to 1 cm. In general, the prior values were positively biased, while the posterior estimates are relatively unbiased. The posterior RMSE values for snow pillows range from 5 to 18 cm (11 cm across all sites). The posterior correlation coefficient values for snow pillows range from 0.91 to 0.99 (0.97 across all sites). The results are qualitatively similar

for snow courses, with uniform and significant improvement in all metrics across all basins (with posterior ME, RMSE, and correlation coefficient across all sites of 23 cm, 13 cm, and 0.95 respectively). Scatterplots showing the comparison of posterior estimates to observations are shown in Figure 1 and visually confirm the general agreement between the posterior estimates and observations. It should be reiterated that the comparison to snow pillow and course data has weaknesses in that the sites generally under sample sloped and forested conditions and are thus potentially no representative of grid-averaged estimates. Nonetheless, the accuracy of the SWE reanalysis estimates does not vary significantly across watersheds, despite forest fraction ranging nearly an order of magnitude.

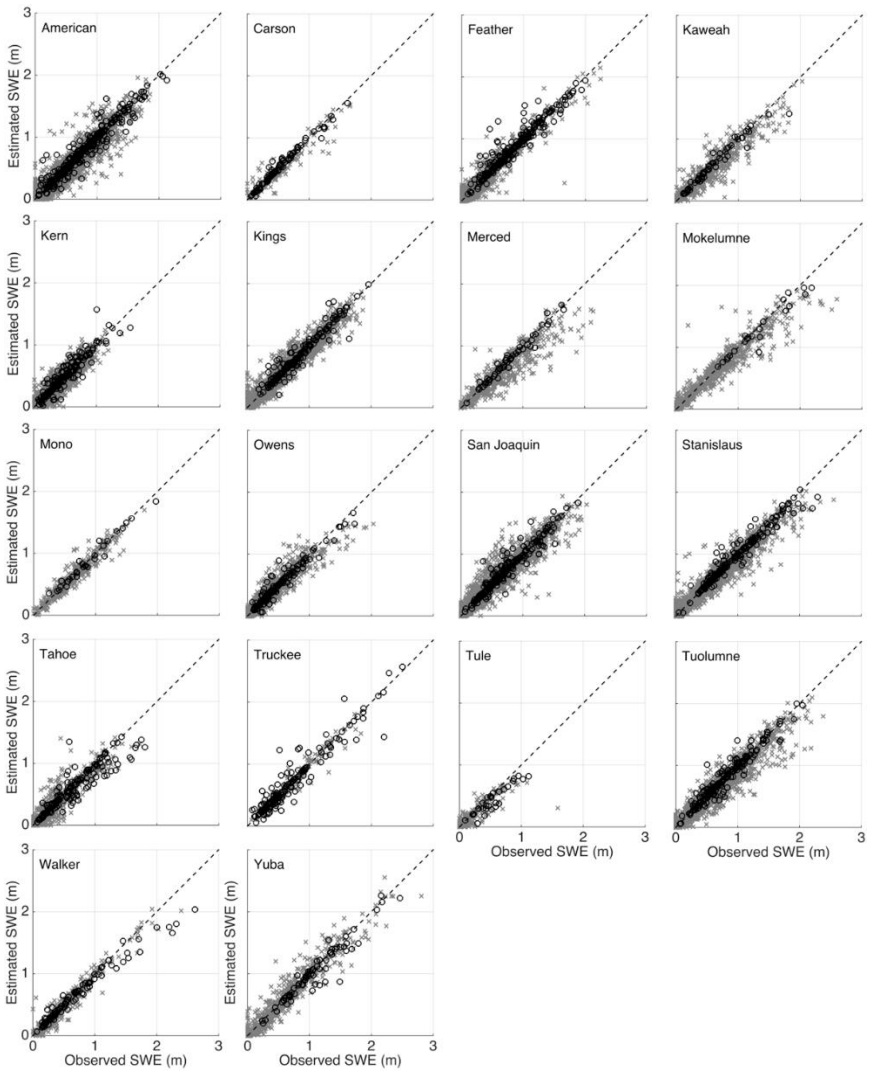

Figure 1. Comparison of observed peak SWE at snow pillow (black 'o' symbols) and snow course (grey 'x' symbols) locations to posterior SWE reanalysis estimates.

Climatology of the Sierra Nevada

Pixel-wise Climatology

Figures 2a show the climatological (31-yr average, from 1984 to 2015) maps of pixel-wise peak SWE. The pixel-wise peak SWE generally shows the highest values at high elevations and on the windward (western) side of the range. The 31-yr average integrated pixel-wise peak SWE volume over the full Sierra Nevada range is 20.0 km^3. The pixel-wise peak SWE is an important metric in that it represents the maximum available water across the season rather than just a snapshot of the SWE at a specified time. This is not only relevant to water resources, but vegetation in water-limited regimes will generally be sensitive to the locally available amount of water from snowmelt (Trujillo et al. 2012), which is a strong function of elevation.

Examples of the 31-years spatiotemporal patterns in interannual variability in pixel-wise peak SWE are illustrated in Fig. 2b-d, where the absolute anomalies relative to the 31-yr climatology are mapped for three of the 31-years. The anomalies for the entire 31-year record can be found in Margulis et al., 2016a. Many of the large-scale dry and wet years anomalies have either uniformly positive or negative anomalies over the full Sierra Nevada range, indicating the effects of large-scale atmospheric phenomena. This is for example the case of the wettest and driest years on record, years 1993 and 2015, respectively (Figure 2cd). Many of the other years show spatial variance in SWE anomalies across the range, which may be indicative of more local-scale processes (e.g., orographic processes and anomalous temperatures) and/or shifts in the storm track that lead to variations in local precipitation and snow accumulation. For example, water year 1999 (Figure 2b) exhibits a relatively uniform south–north gradient with negative anomalies in the southern basins, minimal anomalies in the central basins, and positive anomalies in the northern basins. At least some of this interannual variability is likely due to variations in the number of atmospheric river (AR) and Pineapple Express (PE) events that occurred in a given year.

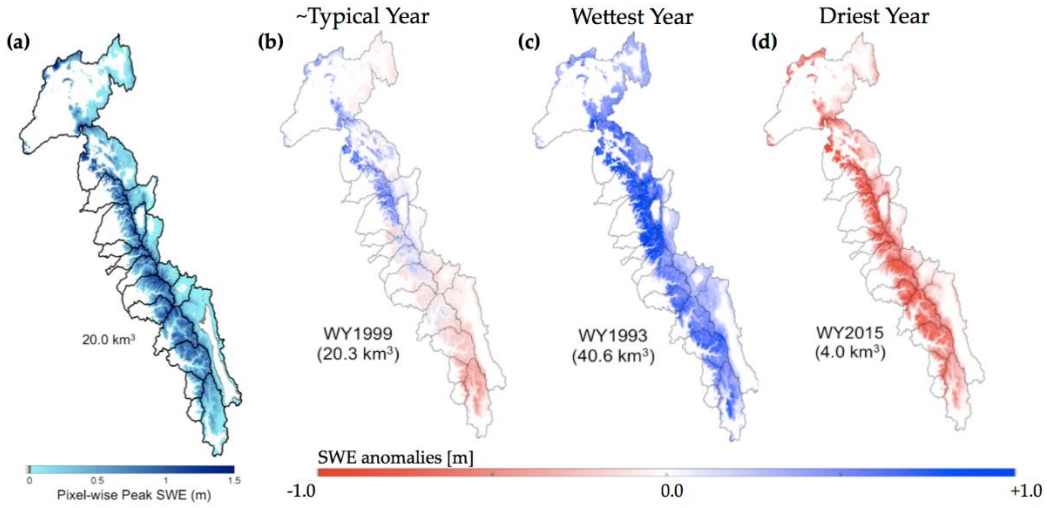

Figure 2. (a) Maps of 31-yr average climatology of pixel-wise peak SWE (m); (b) water year 1999; (c) water year 1993; (d) water year 2015 maps of pixel-wise peak SWE anomalies (m) relative to the 31-yr average pixel-wise peak SWE (shown in panel (a)). Values in parentheses represent the annual integrated storage based on the pixel-wise peak SWE for the corresponding year.

Sierra Nevada Range-wide Climatology

Figure 3 provides a comprehensive illustration of the range-wide SWE data set as a function of both water year and day of water year. The strong seasonal cycle and interannual variability are evident in the data set, which shows a range in the peak SWE from 2.9 to 37.9 km^3 with an average of 18.6 km^3. It is also clear from Figure 3 that the timing of peak SWE varies significantly. While the average day of range-wide peak SWE is 15 March, the interannual day-of-peak ranges from 20 January to 9 May. Considering the actual date of peak is important, as illustrated by 2015, where the peak is quite early (10 February) and much of the snow is melted by 1 April. Hence, using 1 April to quantify variations in peak SWE has the potential to introduce significant errors [Montoya et al., 2014; Margulis et al., 2016a] and in the case of 2015 makes what is already an extreme year seem even more so.

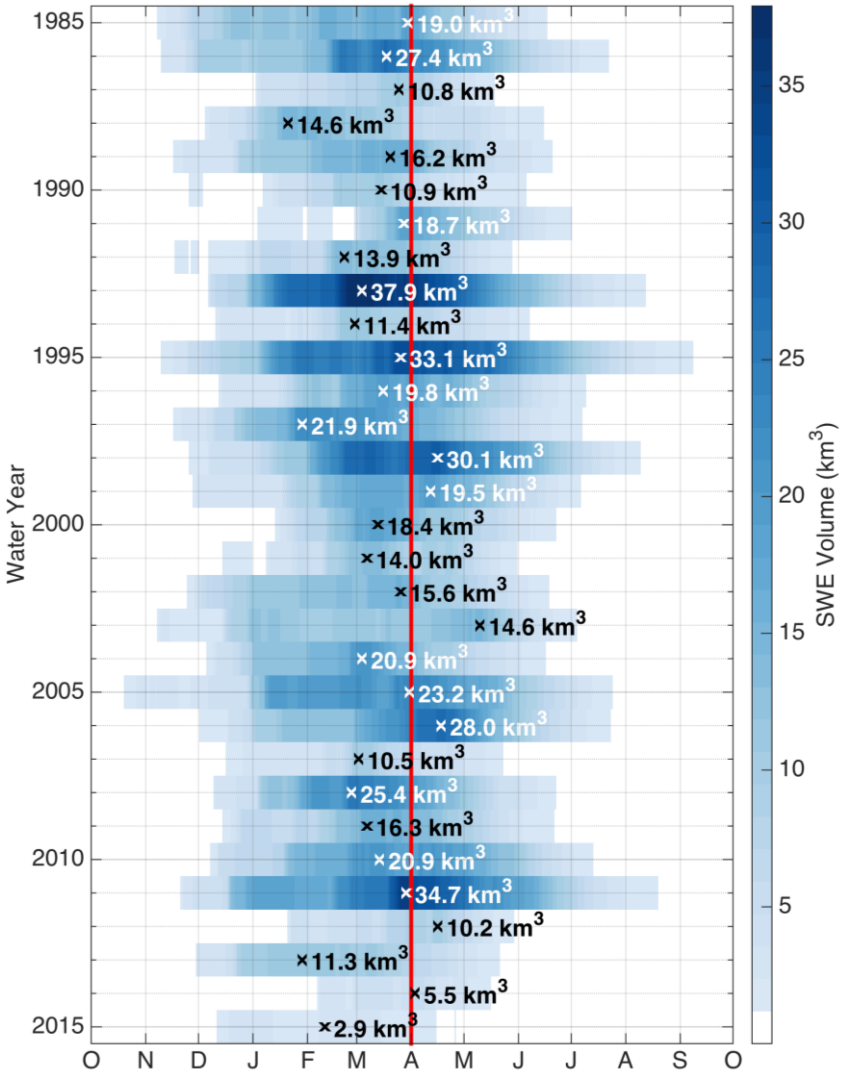

Figure 3. Daily time series of range-wide SWE (in km^3) for each year of the record. The "cross" symbols mark the timing of the peak range-wide SWE for each year, and the corresponding text indicates the value of peak SWE. Above- and below-average values are shown in white and black text, respectively. The red line corresponds to 1 April.

Characterizing the 2015 Snowpack Drought

Extreme Nature of the 2012-2015 Drought

Details on the analysis about the extreme nature of the 2012-2015 snowpack drought can be found in Margulis et al., 2016b. Only a few points are discussed here.

In order to characterize the 2015 drought condition, we extend the widely used Standardized Precipitation Index (SPI) [World Meteorological Organization (WMO), 2012] to an analogous "Standardized SWE Index" (SSI) and build on previously developed concepts for deficit (e.g., Van Loon et al., 2014; Borgomeo et al., 2015), herein applied to annual range-wide peak SWE, to assess the intensity and temporal recovery from a snowpack drought. The SSI can not only be used to diagnose drought or non-drought years, but equally importantly, the fitted probability distribution can be used to assess the return period of the peak annual SWE value for a given year and assess annual SWE variability in a probabilistic context. For fitting a probability distribution to the Sierra Nevada range-wide peak annual SWE time series, we used the merged time series as described in (Supportive information, text S1 in Margulis et al., 2016b). The empirical cumulative distribution function (CDF) from the time series and fitted Gamma CDF are shown in Figure 4. The return period for the 2015 range-wide peak SWE value was found to be 682 years (with a 95% confidence range between 107 and 4356 years). Hence, while the predicted return period is large, it is also highly uncertain based on the parameter uncertainty as a result of the relatively short record and typically few data points in the tails of the distribution.

The return period for 2015 was also analyzed as a function of elevation by fitting a different Gamma distribution to the 31-year reanalysis to SWE in each of the elevation bins. The 2015 return period is a strong function of elevation (Figure 4b). At low elevations (between 1500 and 2100 m) the return period is relatively uniform and high (~1000 year return period). There is a strong transition between 2100 and 3100 m, above which (between 3100 and 3800 m) the return period is also relatively uniform, but much lower (~30 year return period). Again, it should be noted that due to the relatively short record, the uncertainty in these return periods is high, but in any case, the 2015 SWE represents an extreme year relative to the historical record analyzed. While 2015 was an unusual event across all elevations, it was particularly extreme at the lower elevations of the range, most likely due to the extremely warm temperatures that would cause less snowfall and more melt at lower elevations.

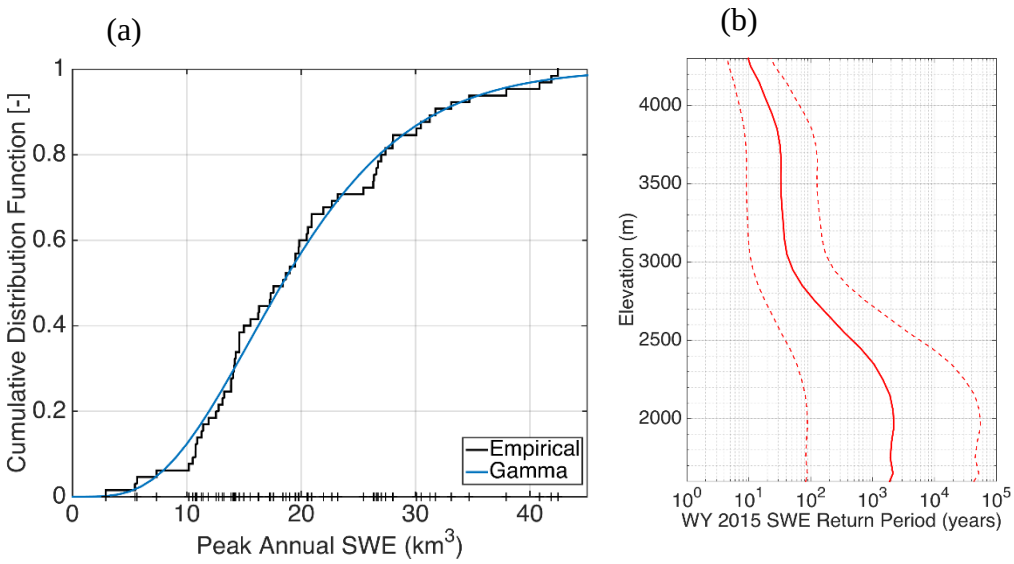

Figure 4. (a) Empirical cumulative distribution function (CDF) of peak annual range-wide SWE (black line) along with the fitted Gamma CDF (blue line). (b) Distribution of return period of 2015 SWE volume for each elevation band (solid red line), and the 95% confidence bounds (dashed red lines).

Prospect of Recovery from the 2012-2015 Drought

To analyze the aggregated intensity of a snowpack drought and its temporal response, we define the annual deviation relative to drought conditions as $d_t = SWE_t - SWE_{drought}$; where $SWE_{drought}$ is a specified threshold defining drought conditions in a given year. The threshold is commonly specified as the value equivalent to a certain percentile. Herein, we link it to the SSI drought threshold. Based on d_t, positive or negative deviation values correspond, respectively, to nondrought or drought conditions in a given year. The cumulative drought deficit over time is defined recursively as $D_t = min[D_{t-1} + d_t; 0]$. In summary, the SWE deviation (d_t) is used to define a "drought year," while the deficit (D_t) is used to classify a "drought period" (i.e., as any continuous period of time with negative values of D). The definition of the deficit D is a generalization of previous work, where allowing for positive annual values of d provides a basis for quantifying the response (recovery) time scale of the drought. By generalizing drought as expressed in terms of d and D, we are acknowledging the fact that a long and intense multiyear drought, leading to large negative values of D, will likely have implications for a much longer recovery than a shorter or less intense drought and that a drought period will not necessarily end upon the first year with conditions greater than a defined threshold. The drought deficit index defined here is strictly applied to snowpack drought but implicitly encompasses downstream impacts in the sense that since snowmelt runoff is such a large fraction of the water supply, when it is unavailable, other sources (e.g., groundwater) may be used to make up the difference.

Figure 5 shows the year-to-year variations in SWE deviations d over the full record along with the evolution of drought deficit D. The 65-year record has 14 drought years as shown with the red bars in Figure 6. The largest drought events in terms of accumulated deficit were those peaking in 1977 (~ 13 km^3) and 2015 (~ 22 km^3), where the deficit ending in 2015 is the largest on record by a significant margin. Aside from these drought events, all others over the record had a deficit between 0 and 2.5 km3. Almost all of the drought events recovered to predrought conditions (i.e., D = 0) in 1 year. For instance, the large deficit year of 1977 ended due to a large positive deviation in 1978. However, in 1987, despite a relatively small drought deficit (2.2 km^3), the drought did not end (i.e., D did not reach zero) in the following year due to a relatively small positive deviation. Hence, the ending of a drought event is partly a function of the starting deficit, but random due to the probabilistic nature of the annual peak SWE time series. This raises the question: given the historically large drought deficit in 2015, what are the prospects of the drought ending going forward?

To project potential snowpack drought recovery, the model for drought deficit (d) and (D) can be combined with a probability distribution fitted to the annual peak SWE time series (i.e. Figure 4a) as part of the SSI construction. Assuming uncorrelated peak SWE from year-to-year, a realization of a time series of peak SWE out to N years into the future can be generated from the Gamma fitted distribution to predict a realization of the evolution of drought from any starting deficit D. A Monte Carlo approach can be taken using many (i.e., 10,000) equally likely realizations to construct a probabilistic representation of the drought deficit evolution going forward. Figure 6 shows the results of the Monte Carlo analysis projecting the drought deficit forward 5 years beyond 2015 with the observed starting deficit of ~ 22 km3. Thus, the likely evolution of the drought period moving forward over the next several years from the deficit estimated at the end of WY 2015 if found to be over 4 years.

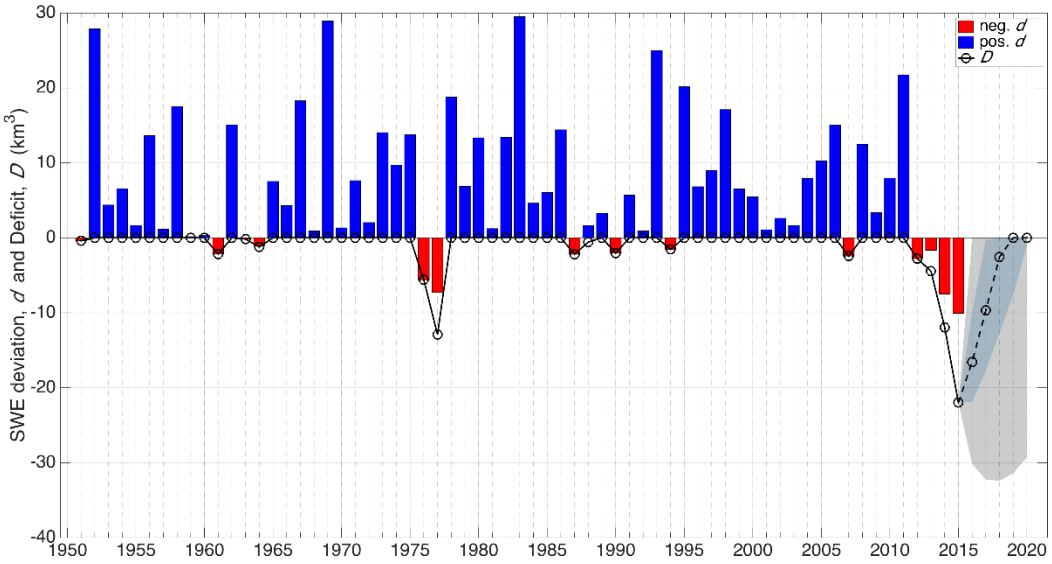

Figure 5. Time series of annual peak SWE deviations (*d*) and cumulative drought deficit (*D*). The projected ensemble median using Monte-Carlo simulation is shown by the black dashed line while the dark grey and light grey bands represent the inter-quartile and 1st-99th percentile ranges respectively.

CONCLUSIONS

This work presents a newly developed state-of-the-art snow reanalysis dataset over the Sierra Nevada based on the assimilation of remotely sensed fSCA over the Landsat 5–8 record (WYs 1985–2015). The new dataset provides a unique capability for investigating snow processes at a resolution (daily and 90m), temporal extent (31 years), and accuracy not available from other existing datasets. Results presented herein provide the first accounting of average annual SWE storage and interannual variability over a large regional mountain range using an advanced (Bayesian) reanalysis (smoothing) approach.

Results found that the pixel-wise peak SWE is on average 20.0 km^3 with significant interannual variability (ranging from a low of 4.0 up to 40.6 km^3). The lowest value in the record (water year 2015) has occurred within the recent and ongoing drought in California. The spatial variability in interannual anomalies in pixel-wise peak SWE is complex in some years with mixed positive and negative anomalies across elevational and spatial gradients.

Further, the results presented herein illustrate the extreme (dry) nature of stored SWE volume in 2015 in the Sierra Nevada, which was shown to have a predicted return period of ~680 years (with a relatively large 95% confidence interval of 107–4356 years due to the 65 year record analyzed). Analysis indicated that in 2015 there was a sharp contrast in return period as function of elevation, with lower elevations having a return period of ~1000 years and higher elevations having a return period of ~30 years. The 2015 peak SWE deviation was the fourth consecutive year of drought, leading to a historically large accumulated multiyear snowpack deficit. Using a Monte Carlo analysis with a fitted probability model, it was shown that the drought period at the end of WY 2015 is very unlikely to be fully alleviated in 2016 (less than 7% probability), and that the expected time scale of recovery to pre-drought conditions is over 4 years.

REFERENCES

Bales, R.C., N.P. Molotch, T.H. Painter, M.D. Dettinger, R. Rice, J. Dozier, 2006: Mountain hydrology of the western United States, *Water Resour. Res.*, 42, W08432, doi:10.1029/2005WR004387.

Belmecheri, S., F. Babst, E.R. Wahl, D.W. Stahle and V. Trouet (2016), Multi-century evaluation of Sierra Nevada snowpack. *Nature Climate Change*, 6(1), 2-3.

Borgomeo, E., G. Pflug, J.W. Hall and S. Hochrainer-Stigler (2015), Assessing water resource system vulnerability to unprecedented hydrological drought using copulas to characterize drought duration and deficit, *Water Resour. Res*., 51, 8927–8948, doi:10.1002/2015WR017324.

Christian-Smith, J., M. C. Levy, and P. H. Gleick (2014), Maladaptation to drought: A case report from California, USA, *Sustainability Sci*., 9(3), doi:10.1007/s11625-014-0269-1.

Cortés, G., M. Girotto, S. Margulis, 2014: Analysis of minimum glacier and snow extent over the Andes using historical Landsat imagery, *Rem. Sens. Environ.*, doi: 10.1016/j.rse.2013.10.023.

Dettinger, M. D. (2013), Atmospheric rivers as drought busters on the US West Coast. *Journal of Hydrometeorology*, 14(6), 1721-1732.

Famiglietti, J. S. (2014), The global groundwater crisis, *Nature Climate Change*, 4(11), 945-948.

Girotto, M., Cortés, G., Margulis, S. A., and M. Durand, 2014: Examining spatial and temporal variability in snow water equivalent using a 27 year reanalysis: Kern River watershed, Sierra Nevada. *Water Resour. Res.*, *50*(8), 6713-6734.

Liston, G. E., 2004: Representing subgrid snow cover heterogeneities in regional and global models, *J. Clim*., 17(6), 1381–1397.

Lundquist, J. D., J. R. Minder, P. J. Neiman, and E. Sukovich, 2010: Relationships between barrier jet heights, orographic precipitation gradients, and streamflow in the northern Sierra Nevada, *J. Hydrometeorol.*, 11(5), 1141–1156.

Mao, Y., B. Nijssen, and D. P. Lettenmaier, 2015: Is climate change implicated in the 2013–2014 California drought? A hydrologic perspective, *Geophys. Res. Lett*., 42, 2805–2813, doi:10.1002/2015GL063456.

Margulis, S., M. Girotto, G. Cortés, and M. Durand, 2015: A Particle Batch Smoother Approach to Snow Water Equivalent Estimation, *J. Hydrometeor*., 16, 1752-1772, doi:10.1175/JHM-D-14-0177.1.

Margulis, S., G. Cortés, M. Girotto, and M. Durand (2016a), A Landsat-era Sierra Nevada (USA) Snow Reanalysis (1985-2015), *J. Hydrometeor*., doi:10.1175/JHM- D-15-0177.1, in press. (early online release: http://journals.ametsoc.org/doi/pdf/10.1175/JHM-D-15-0177.1).

Margulis, S. A., Cortés, G., Girotto, M., Huning, L. S., Li, D., & Durand, M. (2016b). Characterizing the extreme 2015 snowpack deficit in the Sierra Nevada (USA) and the implications for drought recovery. *Geophysical Research Letters*, *43*(12), 6341-6349.

Montoya, E. L., J. Dozier, and W. Meiring, 2014: Biases of April 1 snow water equivalent records in the Sierra Nevada and their associations with large-scale climate indices, *Geophys. Res. Lett., 41,* 5912–5918, doi:10.1002/2014GL060588.

Painter, T. H., J. Dozier, D.A. Roberts, R.E. Davis, and R.O. Green, 2003: Retrieval of subpixel snow-covered area and grain size from imaging spectrometer data. *Remote Sensing of Environment*, *85*(1), 64-77.

Stewart, I. T., D.R. Cayan, and M.D. Dettinger (2004), Changes in snowmelt runoff timing in western North America under a business as usual climate change scenario, *Climatic Change*, *62*(1-3), 217-232.

Trujillo-Gomez, E., N. P. Molotch, M. L. Goulden, A. E. Kelly, and R. C. Bales, 2012: Elevation-dependent influence of snow accumulation on forest greening, *Nat. Geosci*., 5(10), 705–709.

van Loon, A.F., E. Tijdeman, N. Wanders, H. van Lanen, A. Teuling, R. Uijlenhoet (2014), How climate seasonality modifies drought duration and deficit, *J. Geophys. Res.: Atmos*., 119 (8), 4640–4656, doi.10.1002/2013JD020383.

WMO (World Meteorological Organization) (2012), Standardized Precipitation Index User Guide, WMO-No. 1090, 24pp. (http://www.wamis.org/agm/pubs/SPI/WMO_1090_EN.pdf).

Xue, Y., S. Sun, D. S. Kahan, and Y. Jiao, 2003: Impact of parameterizations in snow physics and interface processes on the simulation of snow cover and runoff at several cold region sites, *J. Geophys. Res*., 108(D22), 8859, doi:10.1029/2002JD003174.